Inorganic Chemistry
Article
Cite This: Inorg. Chem. 2019, 58, 411−418
pubs.acs.org/IC

Lanthanides with Unusually Low Oxidation States in the PrB_3^- and PrB_4^- Boride Clusters

Xin Chen,[†,∥] Teng-Teng Chen,[‡,∥] Wan-Lu Li,[†] Jun-Bo Lu,[†] Li-Juan Zhao,[†] Tian Jian,[‡] Han-Shi Hu,[†] Lai-Sheng Wang,*[,‡] and Jun Li*[,†,§]

[†]Department of Chemistry and Key Laboratory of Organic Optoelectronics & Molecular Engineering of Ministry of Education, Tsinghua University, Beijing 100084, China

[‡]Department of Chemistry, Brown University, Providence, Rhode Island 02912, United States

[§]Department of Chemistry, Southern University of Science and Technology, Shenzhen, Guangdong 518055, China

Supporting Information

ABSTRACT: Lanthanide elements typically exhibit a +III oxidation state (OS) in chemical compounds with a few in +IV or even +V OS. Although lanthanides with +II OS have been observed recently in organometallic compounds, +I OS is extremely rare. Using a joint photoelectron spectroscopy and quantum theoretical study, we have found two low OS lanthanides in doped boron clusters, PrB_3^- and PrB_4^-. These two clusters are shown to have planar structures, in which the Pr atom is bonded to the aromatic boron clusters via two Pr−B σ bonds. Chemical bonding and electronic structure analyses reveal that the Pr atom is in a very low OS in the two boride clusters: +II in PrB_3^- and +I in PrB_4^-. The current finding suggests that there should exist a whole class of boride complexes featuring rather low-valent lanthanides and expands the frontier of lanthanide chemistry.

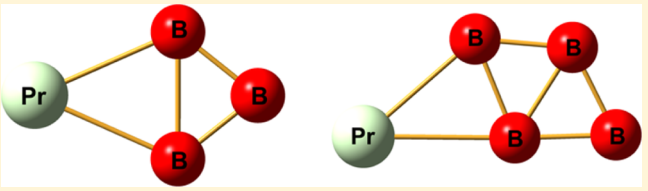

1. INTRODUCTION

Oxidation state (OS) is a highly useful concept in chemical science as well as in the teaching of chemistry. The discovery of new and unusual OS for chemical elements has been of great interest in chemistry and materials science. The highest OS in neutral compounds is +VIII, only occurring in a few MO_4 (M = Ru, Os, Ir, Xe) oxides.[1−7] The only known compound with +IX OS is the gaseous IrO_4^+ cation, as recently verified both theoretically and experimentally.[8,9] Subsequently, Yu and Truhlar suggested a rare Pt(X) species in PtO_4^{2+} using single-reference calculations with density functional theory (DFT).[10] However, more extensive calculations with open-shell singlet DFT and multireference ab initio wavefunction theory have proved very recently that the Pt(X) species is extremely high in energy and the PtO_4^{2+} cation is unlikely to be stable in ambient conditions.[11]

The 4f orbitals in lanthanides (Ln) are rather contracted radially[12] and usually do not participate in chemical bonding unless in molecules with extremely short multiple-bond distances.[13] The more favorable and common OS for the lanthanides is +III, though high-valent +IV OS is also known for Ce, Pr, Nd, Tb, and Dy.[14] Recent experimental and theoretical studies have shown that pentavalent lanthanides can exist in, for instance, PrO_4, PrO_2^+, NPrO, and $NPrO^-$,[13,15] and OS of +II can be found in all lanthanides.[16−21] Therefore, lanthanide compounds with OS = +II, +III, +IV, and +V have all been identified thus far. However, monovalent Ln(I) species are still quite rare except in diatomic halide molecules.[22]

Recently, we have studied a lanthanide-doped boron cluster, PrB_7^-, and found the rare Pr(II) OS in a half-sandwich Pr(II)[η^7-B_7^{3-}] complex,[23] in which the Pr(II) center is coordinated by an aromatic quasiplanar B_7^{3-} ligand. The low electronegativity of boron and the aromatic stabilization of boron clusters provide unique opportunities to tune the lanthanide OS via rational design. Here, we report a joint photoelectron spectroscopy (PES) and quantum chemistry study on two small Pr boride clusters, PrB_3^- and PrB_4^-, to search for even lower Ln OS. We find that the B_3^- and B_4^- clusters formally accept two and one electron, respectively, upon bonding with the Pr atom, forming $[Pr^{II}][B_3^{3-}]$ and $[Pr^{I}][B_4^{2-}]$ species. The optimal structures of PrB_3^-, PrB_4^-, and their corresponding neutrals are shown in Figure 1. The latter is the first monovalent Ln(I) boride compound observed experimentally.

2. METHODS

2.1. Experimental Details. Figure 2 shows the PE spectra of PrB_3^- and PrB_4^-. The experiment was done with a magnetic-bottle-type PES apparatus equipped with a laser vaporization supersonic cluster source and a time-of-flight mass spectrometer, details of which have been published elsewhere.[24,25] Briefly, both the PrB_3^- and the PrB_4^- clusters were produced by laser ablation of a Pr/^{11}B composite target followed by supersonic expansion with a He carrier gas containing 5% argon. Various PrB_n^- clusters were produced and the PrB_3^- and PrB_4^- clusters of current interest were mass-selected and

Received: September 10, 2018
Published: December 13, 2018

DOI: 10.1021/acs.inorgchem.8b02572
Inorg. Chem. 2019, 58, 411−418

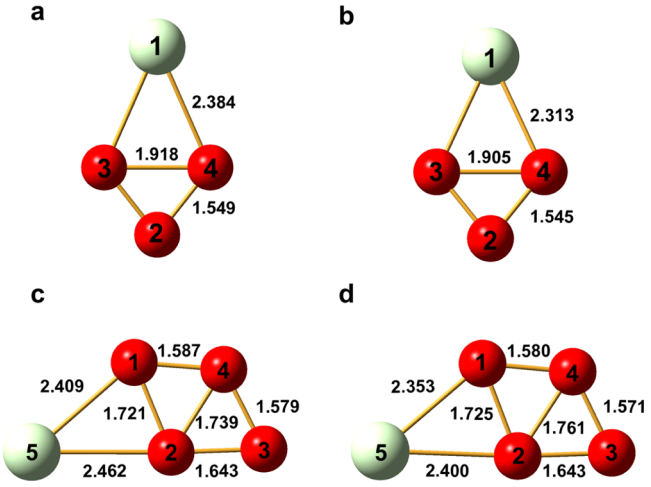

Figure 1. Global minimum structures for (a) PrB_3^- (C_{2v}, $^4A_2$), (b) PrB_3 (C_{2v}, $^3A_2$), (c) PrB_4^- (C_s, $^3A'$), and (d) PrB_4 (C_s, $^4A'$) at the PBE0/TZP level. The bond lengths are given in Å.

decelerated before photodetachment by the 193 nm (6.424 eV) radiation from an ArF excimer laser. The photoelectron spectra were calibrated using the known spectrum of Bi^-. The energy resolution of the apparatus was about 2.5%, that is, around 25 meV for 1 eV electrons.

2.2. Computational Details. The constraint Basin-Hopping algorithm-based Tsinghua Global Minimum 2 (TGMin-2) program[26−28] was used to search for the global minima of PrB_3^- and PrB_4^-. The Amsterdam Density Functional program (ADF 2016.101)[29] with the Perdew-Burke-Ernzerhof (PBE) functional[30] and the polarized triple-zeta (TZP) basis set[31] was used for structural optimization. Vibrational frequencies were calculated at the same level. For both clusters, the frozen-core approximation was used for the inner shells, that is, $[1s^2]$ for B and $[1s^2-4d^{10}]$ for Pr. The scalar relativistic effects were taken into account by the zero-order-regular approximation.[32]

Figure S1 shows the stable isomers found for PrB_3^- and PrB_4^- by using the TGMin code. The isomers were further optimized using DFT at the hybrid PBE0/TZP level.[33] Ab initio RHF-ROCCSD(T)[34] single-point calculations using MOLPRO 2012[35] were performed to evaluate the electron configurations of the global minimum PrB_3^- [$Pr(s^1f^2, f^3, f^2)$] and PrB_4^- [$Pr(s^2f^2, s^1d^1f^2, s^1f^2)$]. In the RHF-ROCCSD(T) calculations, the valence triple-zeta basis set (cc-pVTZ) was applied for B[36] and the Stuttgart energy-consistent relativistic pseudopotential ECP28MWB with the corresponding ECP28MW-B_ANO basis set was used for Pr.[37−39] Vertical detachment energies (VDEs) were calculated using the ΔSCF-TDDFT approach, as described before.[40] The first VDEs (VDE_1) for PrB_3^- and PrB_4^- were calculated as the difference in energy between the anionic ground state and the corresponding neutral ground state at the optimized anion geometry. Vertical excitation energies of the neutral species calculated using the time-dependent DFT method[41−43] and the SAOP functional (TDDFT−SAOP)[44] were added to VDE_1 to yield the higher VDEs. The first adiabatic detachment energy (ADE_1), calculated only for the global minimum anion isomers, was obtained as the energy difference between the anionic and neutral species at their respectively optimized geometries (Table 1). Adaptive natural density partitioning (AdNDP)[45] results were obtained with Multiwfn-3.4.1[46] using the PBE0/cc-pVTZ/ECP28MWB results from Gaussian 09, revision D.01.[47]

3. RESULTS AND DISCUSSION

3.1. Global Minimum Structures. The optimized geometries for the global minima of PrB_3^-, PrB_4^- and their corresponding neutrals at the PBE0/TZP level are shown in Figure 1. The detailed coordinates of these structures are given

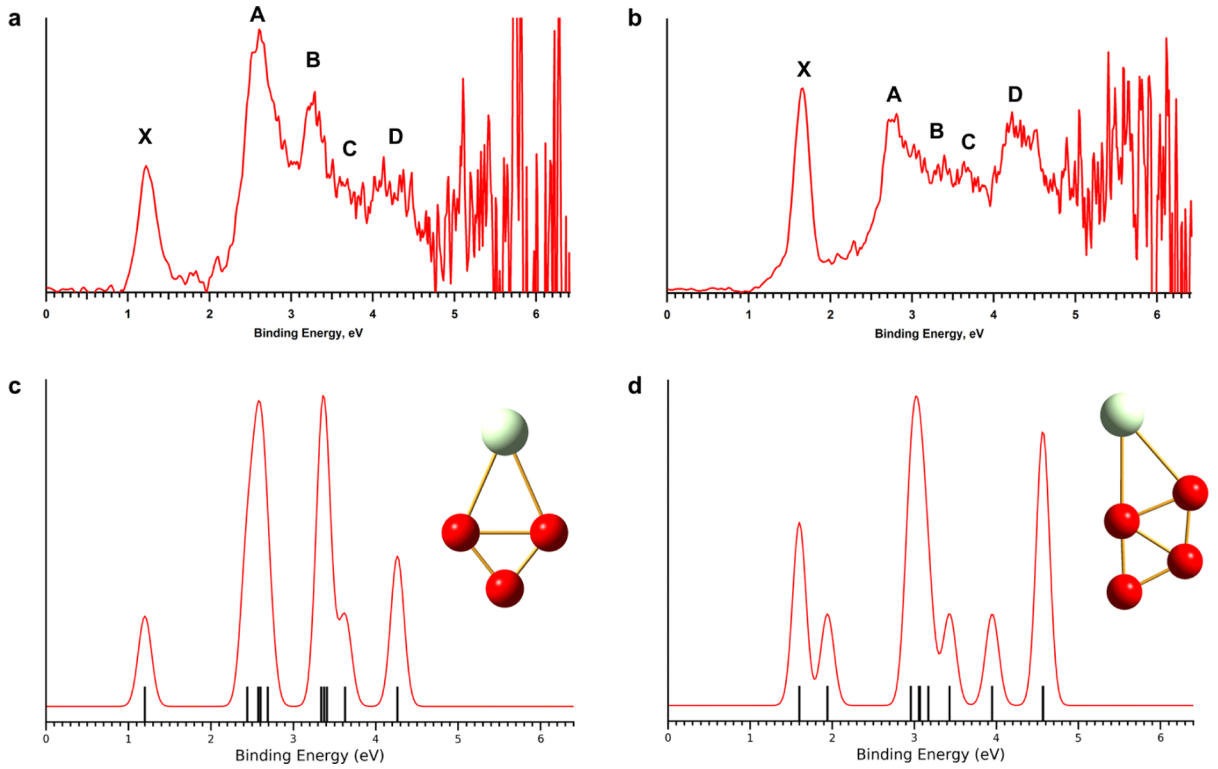

Figure 2. Photoelectron spectrum of PrB_3^- (a) and PrB_4^- (b) at 193 nm. (c,d) are the simulated spectra from the global minima structures of PrB_3^- and PrB_4^- by fitting the calculated VDEs (vertical bars) with a unit area Gaussian function of 0.08 eV half-width. The VDE_1 of PrB_4^- is shifted to align with the X band (see Table 2).

DOI: 10.1021/acs.inorgchem.8b02572
Inorg. Chem. 2019, 58, 411−418

Table 1. Experimental and Theoretical VDE_1 and ADE (eV) of PrB_3^- and PrB_4^-[a]

		exp	PBE0	CCSD(T)
PrB_3^-	ADE_1 (eV)	1.15	1.14	0.86
	VDE_1 (eV)	1.22	1.20	0.90
PrB_4^-	ADE_1 (eV)	1.56	1.43	1.43
	VDE_1 (eV)	1.66	1.50	1.44

[a]The calculated CCSD T1 diagnostics are: 0.043 (PrB_3^-), 0.034 (PrB_3), 0.045 (PrB_4^-), and 0.047 (PrB_4), indicating that accurate calculations of the energies of these systems require multireference ab initio methods.

in Table S1 (PrB_3^- and PrB_3) and Table S2 (PrB_4^- and PrB_4). Both PrB_3^- and PrB_4^- can be seen as substituting one terminal B atom from the planar B_4^- and B_5^- clusters.[48,49] The global minimum of PrB_3^- has a C_{2v} symmetry and a quartet ($^4A_2$) ground electronic state with a pseudoatomic $Pr(s^1f^2)$ configuration. The electronic states with other Pr configurations are higher in energy: f^2 (~20 kcal/mol), f^3 (~27 kcal/mol) at the RHF-ROCCSD(T) level. The global minimum of PrB_4^- is found to have a C_s symmetry and a triplet ground electronic state ($^3A'$) with a $Pr(s^2f^2)$ configuration. A high-spin quintet state ($^5A'$) with a $Pr(s^1d^1f^2)$ configuration is ~9 kcal/mol higher in energy at the RHF-ROCCSD(T) level. The $Pr(s^2f^2)$ configuration means a Pr(I) OS, which is quite unusual in lanthanide chemistry. Hence, we also tested $Pr^{II}(s^1f^2)$, which is ~18 kcal/mol higher at the RHF-ROCCSD(T) level, and $Pr^{III}(f^2)$, which is ~40 kcal/mol higher at the PBE0/TZP level. These results show that the Pr atom favors the unprecedentedly low +I OS in the PrB_4^- cluster. The Kohn–Sham canonical molecular orbitals (MOs) for the global minima of PrB_3^- and PrB_4^- are shown in Figures 3 and 4, respectively, as well as the MOs of the B_3^- and B_4^- moieties in the local coordinate system (LCS, Figure 5).

3.2. Comparison of Experimental and Theoretical Photoelectron Spectra. Figure 2 shows the PE spectra of PrB_3^- and PB_4^-, compared with the simulated spectra from the respective global minima. Each of the two spectra displays a sharp low binding energy band (X) followed by a sizable energy gap. Band X corresponds to the detachment transition from the ground electronic state of the anion (PrB_3^- and PrB_4^-) to the corresponding neutral ground electronic state (PrB_3 and PrB_4), whereas the higher binding energy bands denote detachment transitions to excited electronic states of the neutrals. For PrB_3^- (Figure 2a), band X yields a VDE_1 of 1.22 eV. The first ADE is estimated from the onset of band X to be 1.15 eV, which also represents the electron affinity (EA) of neutral PrB_3. Band A at 2.61 eV is quite strong and broad, followed by a well-defined band B at 3.29 eV. Beyond band B, the spectrum is not well resolved, and bands C and D are labeled for the sake of discussion. For PrB_4^- (Figure 2b), band X gives rise to a VDE_1 of 1.66 eV, and an estimated ADE_1 of 1.56 eV from the band onset, that is the EA of PrB_4. Band A of PrB_4^- with a VDE of 2.81 eV is quite broad. The spectrum of

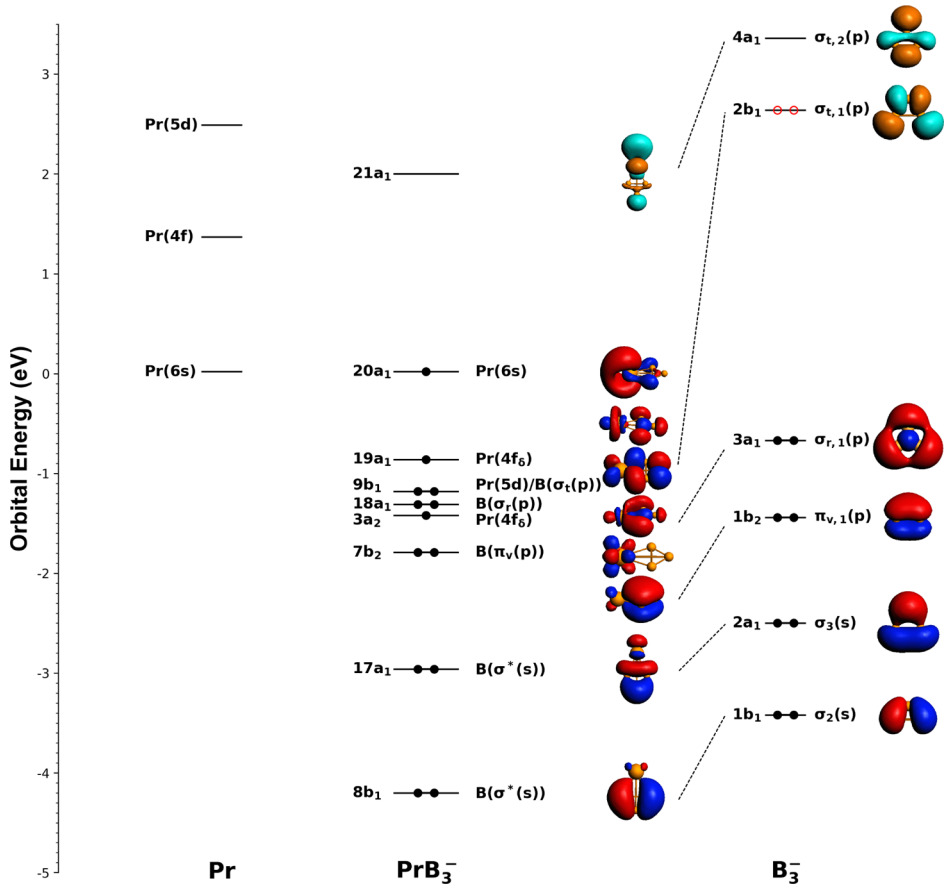

Figure 3. Kohn–Sham molecular orbital energy levels of PrB_3^- and the LCS orbitals of the B_3^- moiety at the PBE0/TZP level. The valence MOs of the B_3^- are divided into four types: $\sigma(s)$, $\sigma_t(p)$, $\sigma_r(p)$, and $\pi_v(p)$. Here "t", "r" and "v" denote tangential, radial, and vertical, respectively. The atomic orbitals of Pr are shifted for clarity.

DOI: 10.1021/acs.inorgchem.8b02572
Inorg. Chem. 2019, 58, 411–418

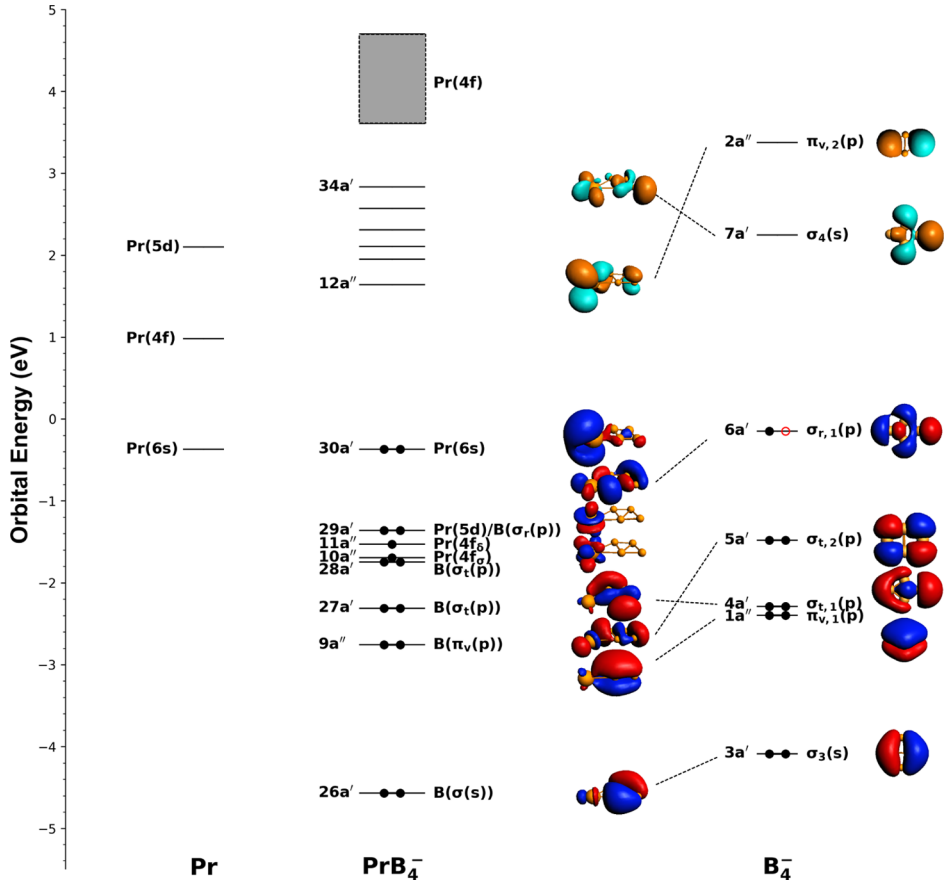

Figure 4. Kohn–Sham molecular orbital energy levels of PrB_4^- and the LCS orbitals of the B_4^- moiety at the PBE0/TZP level. The atomic orbitals of Pr are shifted for clarity.

PrB_4^- at high binding energies is also very complicated and three bands (B, C, D) are tentatively identified. For both spectra, the relatively sharp peak X suggests detachment of a nonbonding electron and very little geometry change between the ground states of the anion and the corresponding neutral. The experimental VDEs of all the observed bands for PrB_3^- and PrB_4^- are given in Table 2, where they are compared with the theoretical data (vide infra).

The calculated VDE_1 and ADE_1 for both PrB_3^- and PrB_4^- at the PBE0/TZP and RHF-ROCCSD(T) levels are given in Table 1. For PrB_3^-, the first electron detachment corresponds to the removal of the single Pr(6s) electron from the relatively diffuse singly occupied MO (SOMO) $20a_1$ (Table 2 and Figure 3). The calculated VDE_1 at the PBE0/TZP level is 1.20 eV, which agrees well with the experimental result (1.22 eV). The resulting neutral state is triplet $^3A_2$, corresponding to an f^2 configuration with Pr in its favorite +III OS, which explains the energy gap following band X and the low EA of PrB_3. The broad band A corresponds to four detachment channels from the Pr–B bonding orbital $9b_1$ and the B–B bonding orbital $18a_1$ (Figure 3): $^5B_2$ at 2.44 eV, $^5A_2$ at 2.58 eV, $^3A_2$ at 2.60 eV, and $^3B_2$ at 2.69 eV (Table 2). Band B comes from electron detachment from the mainly π bonding orbital $7b_2$ of the B_3^- moiety: $^5B_1$ at 3.44 eV and $^3B_1$ at 3.41 eV. Detachment from the primarily Pr(4f) $19a_1$ orbital also contributes to band B: $^3A_2$ at 3.37 eV, though the detachment cross sections for 4f orbitals are usually low. Higher binding energy detachment channels are all from primarily B–B bonding orbitals on the B_3^- moiety.

For PrB_4^-, the first electron detachment also corresponds to the removal of a 6s electron from the closed-shell highest occupied molecular orbital (HOMO) 30a′ (Figure 4), leading to the 4A′ final neutral state with a Pr(f^2s^1) configuration and +II OS. The calculated VDE_1 at the PBE0 level (1.50 eV) is in good agreement with the experiment value of 1.66 eV (Table 1). The corresponding low-spin detachment channel (^{2}A′ at 1.84 eV) from the HOMO 30a′ should also contribute to the X band or the weak signals between bands X and A. The broad band A at about 2.81 eV corresponds to four detachment channels: the Pr–B bonding MO (29a″) (^{4}A′ at 2.86 eV and ^{2}A′ at 2.96 eV) and the two 4f-based SOMO (11a″ and 10a″) giving rise to two ^{2}A″ final states at calculated VDEs of 2.97 and 3.07 eV (Table 2 and Figure 4). The B and C bands are assigned to the low spin states from detachment of 28a′ and 27a′ (two B–B bonding MOs). The high-spin final states from detachment of these two MOs result in similar VDEs, but their weights were low in the TD-DFT calculations, suggesting difficulties of using the single-referenced DFT to describe these states. Band D is mainly from detachment from the π MO (9a″) on the B_4^- moiety (Figure 4); the computed VDE of 4.47 eV is in good agreement with the experimental value of 4.25 eV. Overall, the theoretical results agree well with the experimental data for both clusters, confirming the global minima for PrB_3^- and PrB_4^-, as well as the adequacy of the theoretical methods.

3.3. Oxidation States and Chemical Bonding. The geometry changes from the anion to neutral are similar in the two cluster systems (Figure 1). The Pr–B bonds are noticeably

DOI: 10.1021/acs.inorgchem.8b02572
Inorg. Chem. 2019, 58, 411–418

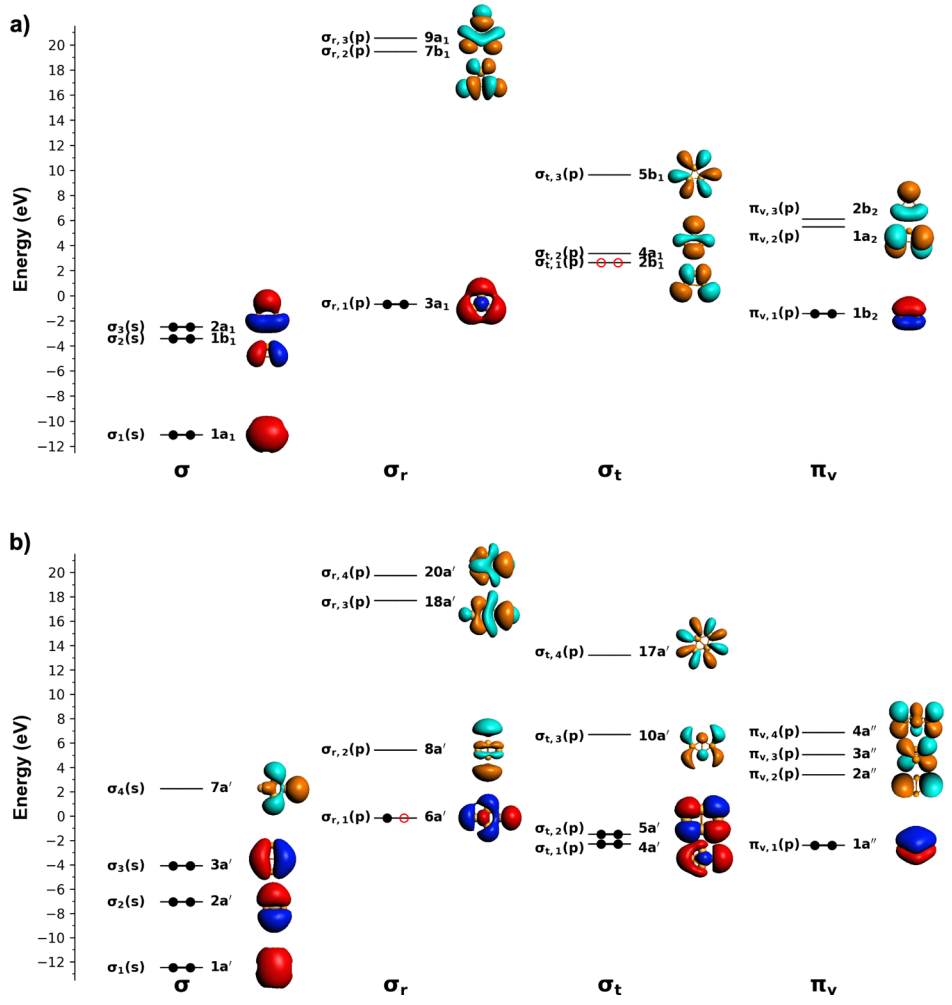

Figure 5. MOs in the LCS of (a) B_3^- moiety and (b) B_4^- at the PBE0/TZP level. The valence MOs of the B_3^- and B_4^- moieties are divided into four types: σ, σ_t, σ_r, and π_v. Here "t" denotes tangential, "r" means radial with regards to the B_x^- ring, and "v" represents vertical. Black dots denote electrons from the B_x^- moiety, whereas additional electrons required are displayed as red dots.

shorter in the two neutrals than those in the anions, mainly because of the increased electrostatic interactions between the Pr center and the boron clusters. The B_3 and B_4 moieties are almost the same from the anions to the neutrals, consistent with the fact that the first detachment channels in both systems come from the diffuse and nonbonding 6s orbitals. Thus, the PrB_3^- anion can be viewed as $Pr^{II}(B_3^{3-})$ and the PrB_4^- anion can be viewed as $Pr^{I}(B_4^{2-})$, whereas the corresponding neutrals can be viewed as $Pr^{III}(B_3^{3-})$ and $Pr^{II}(B_4^{2-})$, respectively. The calculated Mulliken charges and spin distributions of the Pr and B atoms are consistent with the OS assignments, as given in Table S3 (PrB_3^- and PrB_3) and Table S4 (PrB_4^- and PrB_4). Hence, the rare Pr(I) OS exists in the PrB_4^- anion with an electron configuration of f^2s^2, and the Pr in PrB_3^- exists in the low +II OS with a configuration of f^2s^1, as can be seen in the MO diagrams of Figures 3 and 4.

Boron is electron-deficient, and it is therefore surprising that such low OSs exist in the boride clusters. Analyzing the MOs of the B_3^- and B_4^- moieties in the LCS (Figure 5) can help better understand why Pr prefers low OSs in these small boride clusters. Because of the lower electronegativity of Pr compared to B, Pr is expected to lose electrons to the B clusters. The ground state of the B_3^- moiety is a singlet and the HOMO is a $\sigma_{t,1}(p)$ orbital ($2b_1$),[48] where t means the tangential direction along the B_3^- framework. The $\sigma_{t,1}(p)$ and $\sigma_{r,1}(p)$ orbitals, where r denotes the radial direction pointing to the center of the plane, interact with the d orbitals on Pr to form two Pr−B σ bonds (Figure 3). Hence, in PrB_3^-, Pr essentially loses two electrons to the B_3^- moiety, resulting in the Pr^{II} OS. The ground state of B_4^- is doublet and the HOMO (6a′) is singly occupied (Figure 5b).[48] In PrB_4^-, the 5d orbitals on Pr interact with the HOMO and HOMO − 1 to form two Pr−B σ bonds, effectively resulting in the transfer of one electron to B_4^- and the rare Pr^{I} OS. Our RHF-ROCCSD(T) calculations suggest that transferring three electrons from Pr to the B_4^- moiety is not favorable as the $Pr^{III}(f^2)$ configuration is some 20 kcal/mol higher in energy than the $Pr^{I}(s^2f^2)$ configuration.

We further analyzed the chemical bonding in PrB_3^- and PrB_4^- using the AdNDP method (Figure 6).[45] In PrB_3^- the occupation number of Pr is 3.00 |e| (Figure 6a), consisting of one 6s and two 4f electrons in agreement with the +II OS for Pr. The B_3^- moiety consists of two delocalized 3c−2e bonds (σ and π), two peripheral 2c−2e B−B σ bonds, and two 2c−2e Pr−B σ bonds. The AdNDP results for PrB_4^- (Figure 6b) show a 6s long pair and two 4f electrons, consistent with the +I OS for Pr. The B_4^- moiety consists of two 4c−4e delocalized bonds (σ and π), three peripheral 2c−2e B−B σ bonds, and two 2c−2e Pr−B σ bonds. The delocalized σ and π bonds

DOI: 10.1021/acs.inorgchem.8b02572
Inorg. Chem. 2019, 58, 411−418

Table 2. Experimental VDEs of PrB_3^- and PrB_4^- Compared with the Theoretical Data at the TDDFT−SAOP/TZP Level[a]

observed band	VDE (exp)	final state	final-state electron configurations	VDE (theo)
			PrB_3^-	
X	1.22(3)	$^3A_2$	$...(17a_1)^2(7b_2)^2(3a_2)^1(18a_1)^2(9b_1)^2(19a_1)^1(20a_1)^0$	1.20
A	2.61(1)	$^5B_2$	$...(17a_1)^2(7b_2)^2(3a_2)^1(18a_1)^2(9b_1)^1(19a_1)^1(20a_1)^1$	2.44
		$^5A_2$	$...(17a_1)^2(7b_2)^2(3a_2)^1(18a_1)^1(9b_1)^2(19a_1)^1(20a_1)^1$	2.58
		$^3A_2$	$...(17a_1)^2(7b_2)^2(3a_2)^1(18a_1)^1(9b_1)^2(19a_1)^1(20a_1)^1$	2.60
		$^3B_2$	$...(17a_1)^2(7b_2)^2(3a_2)^1(18a_1)^2(9b_1)^1(19a_1)^1(20a_1)^1$	2.69
B	3.29(2)	$^5B_1$	$...(17a_1)^2(7b_2)^1(3a_2)^1(18a_1)^2(9b_1)^2(19a_1)^1(20a_1)^1$	3.34
		$^3A_2$	$...(17a_1)^2(7b_2)^2(3a_2)^1(18a_1)^2(9b_1)^2(19a_1)^0(20a_1)^1$	3.37
		$^3B_1$	$...(17a1)^2(7b2)^1(3a2)^1(18a1)^2(9b1)^2(19a1)^1(20a1)^1$	3.41
C	~3.69	$^3A_1$	$...(17a_1)^2(7b_2)^2(3a_2)^0(18a_1)^2(9b_1)^2(19a_1)^1(20a_1)^1$	3.63
D	~4.13	$^5A_2$	$...(17a_1)^1(7b_2)^2(3a_2)^1(18a_1)^2(9b_1)^2(19a_1)^1(20a_1)^1$	4.26
			PrB_4^-	
X	1.66(1)	$^4A'$	$...(9a'')^2(27a')^2(28a')^2(29a')^2(10a'')^1(11a'')^1(30a')^1$	1.50
		$^2A'$	$...(9a'')^2(27a')^2(28a')^2(29a')^2(10a'')^1(11a'')^1(30a')^1$	1.84
A	2.81(3)	$^4A'$	$...(9a'')^2(27a')^2(28a')^2(29a')^1(10a'')^1(11a'')^1(30a')^2$	2.86
		$^2A'$	$...(9a'')^2(27a')^2(28a')^2(29a')^1(10a'')^1(11a'')^1(30a')^2$	2.96
		$^2A''$	$...(9a'')^2(27a')^2(28a')^2(29a')^2(10a'')^1(11a'')^0(30a')^2$	2.97
		$^2A''$	$...(9a'')^2(27a')^2(28a')^2(29a')^2(10a'')^0(11a'')^1(30a')^2$	3.07
B	3.39(6)	$^2A'$	$...(9a'')^2(27a')^2(28a')^1(29a')^2(10a'')^1(11a'')^1(30a')^2$	3.30[a]
C	3.63(5)	$^2A'$	$...(9a'')^2(27a')^1(28a')^2(29a')^2(10a'')^1(11a'')^1(30a')^2$	3.85[a]
D	~4.25	$^4A''$	$...(9a'')^1(27a')^2(28a')^2(29a')^2(10a'')^1(11a'')^1(30a')^2$	4.47

[a]The VDE_1 is calculated at the PBE0/TZP level. All energies are in eV.

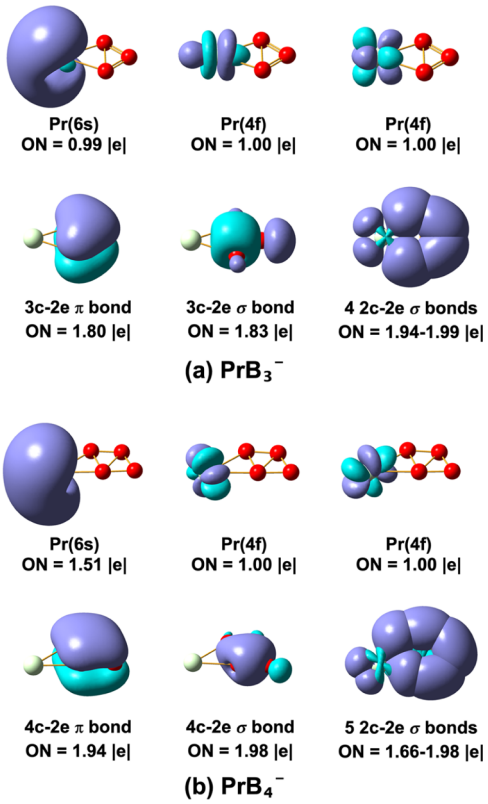

Figure 6. AdNDP bonding analyses for PrB_3^- (a) and PrB_4^- (b) at the PBE0/cc-pVTZ/ECP28MWB level.

render the boron moieties doubly aromatic in both clusters. Hence, PrB_3^- and PrB_4^- each can be viewed as a Pr atom bonded to doubly aromatic boron clusters via two Pr−B covalent bonds, underlying their stabilities relative to other isomers (Figure S1). The stability of the two clusters can also be glimpsed from the large binding energies between Pr and the boron clusters. The calculated binding energy of PrB_3^- ($^4A_2$) → Pr(s^2f^3) + B_3^- ($^1A_1$) is 108.98 kcal/mol and that of PrB_4^- ($^3A'$) → Pr(s^2f^3) + B_4^- ($^2A'$) is 120.83 kcal/mol.

Previous studies on larger lanthanide−boron clusters show that they prefer half-sandwich or inverse-sandwich structures.[23,50,51] In order to explore the geometry preferences of PrB_3^- and PrB_4^-, we computed their relative energy changes as a function of ∠Pr−B_n^- angle θ, as shown in Figure 7. The

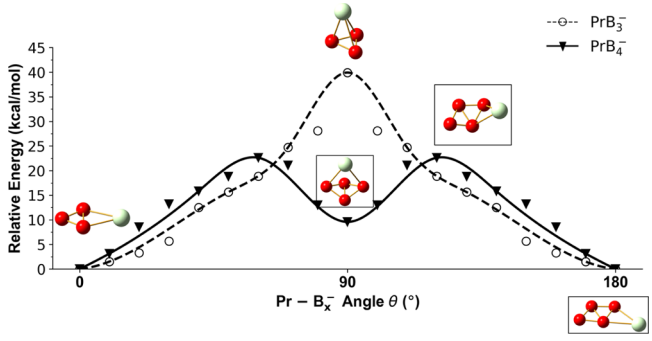

Figure 7. Relative PBE0/TZP energies for PrB_3^- and PrB_4^- as a function of Pr−B_x^- angle θ. For each cluster, the energy for θ = 0° is chosen to be zero.

PrB_3^- cluster becomes more and more unstable as θ increases from 0° (planar) to 90° (half-sandwich), which represents an energy maximum, ~40 kcal/mol higher than the planar structure. The PrB_4^- cluster shows a different trend, for which the half-sandwich structure represents a local minimum, ~10 kcal/mol higher than the planar structure. These observations as well as previous results of SmB_6^- and PrB_7^- suggest that the half-sandwich structures become more energetically favorable when the B_x^- moiety becomes larger.[22,49] Thus, the PrB_5^- and PrB_6^- clusters are likely to

DOI: 10.1021/acs.inorgchem.8b02572
Inorg. Chem. 2019, 58, 411−418

have the planar and half-sandwich structures co-exist, as was the case for SmB_6^-.[50]

4. CONCLUSIONS

In conclusion, we have studied Pr-doped B_3^- and B_4^- clusters using PES and density-functional and ab initio quantum chemical calculations. The global minimum of the PrB_3^- cluster is found to be a planar C_{2v} structure with a Pr^{II} center interacting with a B_3^{3-} moiety. The PrB_4^- cluster is found to have a C_s symmetry with a rare Pr^{I} center interacting with a B_4^{2-} moiety. Both boron moieties exhibit σ and π double aromaticity. The unusually low OS Pr in the boride clusters are interesting, largely owing to the relatively low electronegativity of boron and the stability of the aromatic boron moieties. The current results reveal the possibility of forming unusually low OS for lanthanide elements with boron clusters. The monovalent OS suggests that lanthanide elements can behave like alkali or alkali earth elements in suitable coordination environments, expanding the chemistry of the lanthanides.

■ ASSOCIATED CONTENT

Supporting Information

The Supporting Information is available free of charge on the ACS Publications website at DOI: 10.1021/acs.inorgchem.8b02572.

Coordinates of the PrB_3^- and PrB_4^- isomers at the PBE0/TZP level; calculated Mulliken charges and spin density distributions of $PrB_3^-/PrB_3/PrB_4^-/PrB_4$; and relative energies of the stable isomers of $PrB_3^-$and PrB_4^- at the PBE/TZP, PBE0/TZP levels (PDF)

■ AUTHOR INFORMATION

Corresponding Authors

*E-mail: Lai-Sheng_Wang@brown.edu (L.S.W.).
*E-mail: junli@tsinghua.edu.cn (J.L.).

ORCID

Lai-Sheng Wang: 0000-0003-1816-5738
Jun Li: 0000-0002-8456-3980

Author Contributions

‖X.C. and T.-T.C. contributed equally.

Notes

The authors declare no competing financial interest.

■ ACKNOWLEDGMENTS

The theoretical work at Tsinghua University was supported by the Natural Science Foundation of China (grant nos. 21590792, 91426302, and 21433005). The experimental work at Brown University was supported by the National Science Foundation (CHE-1763380). The calculations were performed using supercomputers at the Tsinghua National Laboratory for Information Science and Technology and the supercomputers of National Supercomputer Center in Guangzhou, China (NSCC-GZ, TianHe II).

■ REFERENCES

(1) Jørgensen, C. K. *Oxidation Numbers and Oxidation States*; Springer: Berlin, 1969.
(2) Gerken, M.; Schrobilgen, G. J. Solution Multi-NMR and Raman Spectroscopic Studies of Thermodynamically Unstable XeO_4. The First ^{131}Xe NMR Study of a Chemically Bound Xenon Species. *Inorg. Chem.* **2002**, *41*, 198−204.
(3) Riedel, S.; Kaupp, M. The highest oxidation states of the transition metal elements. *Coord. Chem. Rev.* **2009**, *253*, 606−624.
(4) Riedel, S. *Comprehensive Inorganic Chemistry II*; Reedijk, J., Poeppelmeier, K., Eds.; Elsevier: Oxford, 2013; Vol. 2.
(5) Huang, W.; Xu, W.-H.; Su, J.; Schwarz, W. H. E.; Li, J. Oxidation States, Geometries, and Electronic Structures of Plutonium Tetroxide PuO_4 Isomers: Is Octavalent Pu Viable? *Inorg. Chem.* **2013**, *52*, 14237−14245.
(6) Huang, W.; Pyykkö, P.; Li, J. Is Octavalent Pu(VIII) Possible? Mapping the Plutonium Oxyfluoride Series PuO_nF_{8-2n} (n = 0−4). *Inorg. Chem.* **2015**, *54*, 8825−8831.
(7) Huang, W.; Xu, W.-H.; Schwarz, W. H. E.; Li, J. On the Highest Oxidation States of Metal Elements in MO_4 Molecules (M = Fe, Ru, Os, Hs, Sm, and Pu). *Inorg. Chem.* **2016**, *55*, 4616−4625.
(8) Wang, G.; Zhou, M.; Goettel, J. T.; Schrobilgen, G. J.; Su, J.; Li, J.; Schlöder, T.; Riedel, S. Identification of an iridium-containing compound with a formal oxidation state of IX. *Nature* **2014**, *514*, 475−477.
(9) Pyykkö, P.; Xu, W.-H. On the Extreme Oxidation States of Iridium. *Chem.—Eur. J.* **2015**, *21*, 9468−9473.
(10) Yu, H. S.; Truhlar, D. G. Oxidation State 10 Exists. *Angew. Chem., Int. Ed.* **2016**, *55*, 9004−9006.
(11) Hu, S.-X.; Li, W.-L.; Lu, J.-B.; Bao, J. L.; Yu, H. S.; Truhlar, D. G.; Gibson, J. K.; Marçalo, J.; Zhou, M.; Riedel, S.; Schwarz, W. H. E.; Li, J. On the Upper Limits of Oxidation States in Chemistry. *Angew. Chem., Int. Ed.* **2018**, *57*, 3242−3245.
(12) Tang, Y.; Zhao, S.; Long, B.; Liu, J.-C.; Li, J. On the Nature of Support Effects of Metal Dioxides MO_2 (M = Ti, Zr, Hf, Ce, Th) in Single-Atom Gold Catalysts: Importance of Quantum Primogenic Effect. *J. Phys. Chem. C* **2016**, *120*, 17514−17526.
(13) Hu, S.-X.; Jian, J.; Su, J.; Wu, X.; Li, J.; Zhou, M. Pentavalent lanthanide nitride-oxides: NPrO and $NPrO^-$ complexes with N≡Pr triple bonds. *Chem. Sci.* **2017**, *8*, 4035−4043.
(14) Su, J.; Hu, S.; Huang, W.; Zhou, M.; Li, J. On the oxidation states of metal elements in MO_3^- (M = V, Nb, Ta, Db, Pr, Gd, Pa) anions. *Sci. China: Chem.* **2016**, *59*, 442−451.
(15) Zhang, Q.; Hu, S.-X.; Qu, H.; Su, J.; Wang, G.; Lu, J.-B.; Chen, M.; Zhou, M.; Li, J. Pentavalent Lanthanide Compounds: Formation and Characterization of Praseodymium(V) Oxides. *Angew. Chem., Int. Ed.* **2016**, *55*, 6896−6900.
(16) Meyer, G. Reduced halides of the rare-earth elements. *Chem. Rev.* **1988**, *88*, 93−107.
(17) Evans, W. J. The Importance of Questioning Scientific Assumptions: Some Lessons from f Element Chemistry. *Inorg. Chem.* **2007**, *46*, 3435−3449.
(18) Palumbo, C. T.; Fieser, M. E.; Ziller, J. W.; Evans, W. J. Reactivity of Complexes of $4f^n5d^1$ and $4f^{n+1}$ Ln^{2+} Ions with Cyclooctatetraene. *Organometallics* **2017**, *36*, 3721−3728.
(19) Ryan, A. J.; Darago, L. E.; Balasubramani, S. G.; Chen, G. P.; Ziller, J. W.; Furche, F.; Long, J. R.; Evans, W. J. Synthesis, Structure, and Magnetism of Tris(amide) $[Ln\{N(SiMe_3)_2\}_3]^{1-}$ Complexes of the Non-traditional +2 Lanthanide Ions. *Chem.—Eur. J.* **2018**, *24*, 7702−7709.
(20) Fieser, M. E.; Palumbo, C. T.; La Pierre, H. S.; Halter, D. P.; Voora, V. K.; Ziller, J. W.; Furche, F.; Meyer, K.; Evans, W. J. Comparisons of lanthanide/actinide +2 ions in a tris(aryloxide)arene coordination environment. *Chem. Sci.* **2017**, *8*, 7424−7433.
(21) Meyer, G. All the Lanthanides Do It and Even Uranium Does Oxidation State +2. *Angew. Chem., Int. Ed.* **2014**, *53*, 3550−3551.
(22) Schoendorff, G.; Wilson, A. K. Low valency in lanthanides: A theoretical study of NdF and LuF. *J. Chem. Phys.* **2014**, *140*, 224314.
(23) Chen, T.-T.; Li, W.-L.; Jian, T.; Chen, X.; Li, J.; Wang, L.-S. PrB_7^- : A Praseodymium-Doped Boron Cluster with a Pr^{II} Center Coordinated by a Doubly Aromatic Planar η^7-B_7^{3-} Ligand. *Angew. Chem., Int. Ed.* **2017**, *56*, 6916−6920.
(24) Wang, L.-S.; Cheng, H.-S.; Fan, J. Photoelectron spectroscopy of size-selected transition metal clusters: Fe_n, n=3−24. *J. Chem. Phys.* **1995**, *102*, 9480−9493.

DOI: 10.1021/acs.inorgchem.8b02572
Inorg. Chem. 2019, 58, 411−418

(25) Wang, L.-S. Photoelectron spectroscopy of size-selected boron clusters: from planar structures to borophenes and borospherenes. *Int. Rev. Phys. Chem.* **2016**, *35*, 69−142.
(26) Zhai, H.-J.; Zhao, Y.-F.; Li, W.-L.; Chen, Q.; Bai, H.; Hu, H.-S.; Piazza, Z. A.; Tian, W.-J.; Lu, H.-G.; Wu, Y.-B.; Mu, Y.-W.; Wei, G.-F.; Liu, Z.-P.; Li, J.; Li, S.-D.; Wang, L.-S. Observation of an all-boron fullerene. *Nat. Chem.* **2014**, *6*, 727−731.
(27) Chen, X.; Zhao, Y.-F.; Wang, L.-S.; Li, J. Recent progresses of global minimum searches of nanoclusters with a constrained Basin-Hopping algorithm in the TGMin program. *Comput. Theor. Chem.* **2017**, *1107*, 57−65.
(28) Zhao, Y.; Chen, X.; Li, J. TGMin: A global-minimum structure search program based on a constrained basin-hopping algorithm. *Nano Res.* **2017**, *10*, 3407−3420.
(29) te Velde, G.; Bickelhaupt, F. M.; Baerends, E. J.; Fonseca Guerra, C.; van Gisbergen, S. J. A.; Snijders, J. G.; Ziegler, T. Chemistry with ADF. *J. Comput. Chem.* **2001**, *22*, 931−967.
(30) Perdew, J. P.; Burke, K.; Ernzerhof, M. Generalized Gradient Approximation Made Simple. *Phys. Rev. Lett.* **1996**, *77*, 3865−3868.
(31) Van Lenthe, E.; Baerends, E. J. Optimized Slater-type basis sets for the elements 1-118. *J. Comput. Chem.* **2003**, *24*, 1142−1156.
(32) van Lenthe, E.; Baerends, E. J.; Snijders, J. G. Relativistic regular two-component Hamiltonians. *J. Chem. Phys.* **1993**, *99*, 4597−4610.
(33) Adamo, C.; Barone, V. Toward reliable density functional methods without adjustable parameters: The PBE0 model. *J. Chem. Phys.* **1999**, *110*, 6158−6170.
(34) Knowles, P. J.; Hampel, C.; Werner, H.-J. Coupled cluster theory for high spin, open shell reference wave functions. *J. Chem. Phys.* **1993**, *99*, 5219−5227.
(35) Werner, H.-J.; Knowles, P. J.; Knizia, G.; Manby, F. R.; Schütz, M. Molpro: a general-purpose quantum chemistry program package. *Wiley Interdiscip. Rev.: Comput. Mol. Sci.* **2012**, *2*, 242−253.
(36) Dunning, T. H., Jr. Gaussian basis sets for use in correlated molecular calculations. I. The atoms boron through neon and hydrogen. *J. Chem. Phys.* **1989**, *90*, 1007−1023.
(37) Dolg, M.; Stoll, H.; Preuss, H. Energy-adjusted ab initio pseudopotentials for the rare earth elements. *J. Chem. Phys.* **1989**, *90*, 1730−1734.
(38) Cao, X.; Dolg, M. Valence basis sets for relativistic energy-consistent small-core lanthanide pseudopotentials. *J. Chem. Phys.* **2001**, *115*, 7348−7355.
(39) Cao, X.; Dolg, M. Basis set limit extrapolation of ACPF and CCSD(T) results for the third and fourth lanthanide ionization potentials. *Chem. Phys. Lett.* **2001**, *349*, 489−495.
(40) Li, J.; Li, X.; Zhai, H.-J.; Wang, L.-S. Au_{20}: A Tetrahedral Cluster. *Science* **2003**, *299*, 864−867.
(41) van Gisbergen, S. J. A.; Snijders, J. G.; Baerends, E. J. Implementation of time-dependent density functional response equations. *Comput. Phys. Commun.* **1999**, *118*, 119−138.
(42) Wang, F.; Ziegler, T. Time-dependent density functional theory based on a noncollinear formulation of the exchange-correlation potential. *J. Chem. Phys.* **2004**, *121*, 12191−12196.
(43) Wang, F.; Ziegler, T. The performance of time-dependent density functional theory based on a noncollinear exchange-correlation potential in the calculations of excitation energies. *J. Chem. Phys.* **2005**, *122*, 074109.
(44) Bernasconi, L. Statistical average of model orbital potentials for extended systems: Calculation of the optical absorption spectrum of liquid water. *J. Chem. Phys.* **2010**, *132*, 184513.
(45) Zubarev, D. Y.; Boldyrev, A. I. Developing paradigms of chemical bonding: adaptive natural density partitioning. *Phys. Chem. Chem. Phys.* **2008**, *10*, 5207−5217.
(46) Lu, T.; Chen, F. Multiwfn: A multifunctional wavefunction analyzer. *J. Comput. Chem.* **2012**, *33*, 580−592.
(47) *Gaussian 09*, Revision D.01; Gaussian, Inc.: Wallingford CT, 2009.
(48) Zhai, H.-J.; Wang, L.-S.; Alexandrova, A. N.; Boldyrev, A. I.; Zakrzewski, V. G. Photoelectron Spectroscopy and ab Initio Study of B_3^- and B_4^- Anions and Their Neutrals. *J. Phys. Chem. A* **2003**, *107*, 9319−9328.
(49) Zhai, H.-J.; Wang, L.-S.; Alexandrova, A. N.; Boldyrev, A. I. Electronic structure and chemical bonding of B_5^- and B_5 by photoelectron spectroscopy and ab initio calculations. *J. Chem. Phys.* **2002**, *117*, 7917−7924.
(50) Robinson, P. J.; Zhang, X.; McQueen, T.; Bowen, K. H.; Alexandrova, A. N. SmB_6^- Cluster Anion: Covalency Involving f Orbitals. *J. Phys. Chem. A* **2017**, *121*, 1849−1854.
(51) Li, W. L.; Chen, T. T.; Xing, D. H.; Chen, X.; Li, J.; Wang, L. S. Observation of highly stable and symmetric lanthanide octa-boron inverse sandwich complexes. *Proc. Natl. Acad. Sci. U.S.A.* **2018**, *115*, E6972−E6977.

DOI: 10.1021/acs.inorgchem.8b02572
Inorg. Chem. 2019, 58, 411−418